A R T I C L E

JCCS
JOURNAL OF THE CHINESE CHEMICAL SOCIETY

Structural studies of silica-supported spinel magnesium ferrite nanorods for photocatalytic degradation of methyl orange

Subiya K. Kazi[1] | **Shaukatali N. Inamdar[2]** | **Dhanraj P. Kamble[3]** | **Kishan S. Lohar[4]** | **Appasaheb W. Suryawanshi[5]** | **Radhakrishnan M. Tigote[1]**

[1]Department of Chemistry, Dr. Babasaheb Ambedkar Marathwada University, Aurangabad, India

[2]Department of Pharmaceutical Chemistry, College of Health Sciences, University of KwaZulu-Natal (Westville), Durban, South Africa

[3]Department of Chemistry, S.B.E.S. College of Science, Aurangabad, India

[4]Department of Chemistry, Shrikrishna Mahavidhyalya, Gunjoti, India

[5]Department of Chemistry, Shri Madhavrao Patil Mahavidhyalaya, Murum, India

Correspondence

Radhakrishnan M. Tigote, Department of Chemistry, Dr. Babasaheb Ambedkar Marathwada University, Sub-campus Osmanabad, Aurangabad, Maharashtra, 413501, India
Email: rmtigote.chemobad@bamu.ac.in

Abstract

A novel, well-designed, silica-supported magnesium ferrite nanorods were successfully developed at room temperature using the co-precipitation method. The synthesized nanorods show an optical band gap of 3.1 eV, with the maximum wavelength absorptive at 334 nm. The average particle size is 36 nm with the FCC crystal structure by the X-ray Diffraction technique (XRD). TGA achieved thermal stability of targeted mesoporous materials at 600°C. Field Emission Scanning Electron Microscopy (FE-SEM) and High-Resolution Transmission Electron Microscopy (HR-TEM) techniques confirm the rod-like structure. Energy Dispersive Spectroscopy (EDS) and X-Ray Fluorescence (XRF) studies reveal the presence of all elements in the composition. The synthesized nanorods are highly magnetic by the vibrating sample magnetometer (VSM) technique, which shows a high coercivity value, that is, $MgFe_2O_4@SiO_2$ is photocatalytically active. From BET analysis, the surface area, pore volume, and pore diameter are 19.2 m^2 g^{-1}, 2.46 cm^3 g^{-1}, and 5.10 nm, respectively. The experimental outcomes predict that the degradation efficiency (79%) of methyl orange dye was accomplished using $MgFe_2O_4SiO_2$ nanorods within 270 min.

K E Y W O R D S

crystalline size, degradation of methyl orange dye, magnetic properties, mesoporous ferrite nanoparticles, optical activity, spinel structure

1 | INTRODUCTION

Nanotechnology has received the most attention in the current decade due to its excellent various novel properties and applications.[1] It has brought a revolution in several areas, such as medicine, health, biology, catalysis, communication, environmental protection, and many other disciplines.[2] They have significant optical, electrical, and magnetic properties whenever metal-doped ferrite has a general formula of $Mg_{x-1}Fe_xO_4$ and has octahedral and tetrahedral sites[3] and

is used in a variety of diseases.[4] The Mesoporous metal ferrites composites are semiconducting materials with an n-type of material, and the shell can be biologically compatible with organic surfactants, gold, silica, SiO_2, polymers, and others. Among the above materials, silica is the best one as a shell due to its being nontoxic, easily dispersed in water, thermostable, and having high biocompatibility.[5–7] In an acidic medium, the SiO_2 shell affords a chemically inert surface that shields nanoparticles from leaching. The silica surface contains silane groups, allowing conjugation of its

surface with various functional materials and the formation of covalent bonds–Si—O—Si—in biological systems.[8] belongs to their amorphous SiO_2 layer, which was mostly grown by hydrolysis and condensation of alkoxysilanes such as tetraethyl orthosilicate (TEOS) with an added acidic or basic catalyst. Materials have been drawn to the opportunity to study the magnetic and photocatalytic properties of mesoporous nanoparticles in confined dimensions as part of core-shell nanostructures.

Recent studies have shown that the separation between magnetic nanoparticles in composite materials and the surface properties of the nanoparticles greatly affect their magnetic properties.[9] Among the core/shell materials, they can also be used to protect medicines or other materials from dissolution or hydrolysis and to strengthen polymeric materials. Silica with spherical morphology from nano to micrometer size can be easily and controllably manufactured.[10] In the case of application, in order to prevent aggregation of the magnetic nanoparticles (MNPs), a protecting shell such as silica is usually used to form a core-shell $NPs@SiO_2$ structure. At the same time, the silica shell can generate a large surface formed of Si-OH groups suitable for modification.[11] After the reactions were completed, ferrites supported nanocatalysts were highly stable, recyclable, and magnetically retrievable.[12] These nanoparticles were synthesized using different methods such as chemical reduction method, hydrothermal method,[13] solid-state method and high energy milling,[14] microemulsions,[15] sol–gel method,[16] microwave method,[17] electrospinning,[18] co-precipitation method,[19] ultrasonic wave assisted and also under visible light irradiation method,[20,21] Stober methods,[22] polymeric precursor method,[23] mechano-chemistry,[24] combustion method,[25] green synthesis,[26] magnetic resonance imaging (MRI),[27] biomagnetic separations,[28,29] in biosensors[30] and biotechnology.[31] Magnesium ferrite materials have a wide range of applications, including cell labeling and sorting, high-density magnetic recording, microwave sensors, electronic devices, high-frequency devices, and radio frequency coils.[32]

However, the biological and biomedical applications of silica-supported magnesium ferrite nanoparticles have received a lot of interest due to their anticancer and antibacterial properties.[33–36] They are widely used to control bacterial pollution and ultimately control many infections.[37] They are observed in many forms, such as thin films,[38] Nanopowders,[35] nanofibers,[39] nanowires,[40] nanospheres, even histoarchitecture geometry particles[41] and cubic spinel-type of structures also.[42] However, due to the longer processing time for their application of magnetic nanoparticles as catalysts, they were used for water purification, controlling air pollution,[43] and many organic transformations as well.[44] Muhammad Yakob[45] developed silica-supported magnesium ferrite nanomaterials that are

nontoxic and biologically compatible with living organisms and are used as photocatalysts in the photocatalytic degradation of drugs[46] and methylene blue dyes.[47] The metal nanoparticles are used for photocatalytic degradation[48–63] and also for selective and aerobic oxidation of benzyl alcohol.[64,65]

Herein, we report that the $MgFe_2O_4@SiO_2$ nanorods are synthesized by a simple co-precipitation method at room temperature. The synthesis is done using magnesium perchlorate, ferric nitrate as a precursor, and hydrazine hydrates as a reducing agent. This technique, however, is one of the simplest, most cost-effective, and most feasible methods for producing high-purity, homogeneous, and crystalline nanorods. The resulting nanorods exhibit a smaller band gap (3.1 eV), are non-hazardous, non-toxic, effectively magnetic, and easily separated from the reaction mixture. Thus, these are photocatalytically active; they do not need any co-catalyst, and the stoichiometric amount is sufficient for complete degradation of dye within 270 min, which is a the great advantage of this work.

2 | RESULTS AND DISCUSSION

The synthesized $MgFe_2O_4@SiO_2$ nanorods were characterized using different techniques, such as the optical properties were studied for the optical band gap of the material using UV Visible spectrophotometer ranging from 200 to 800 nm and the crystal structure, including the particle size, was measured by using X-Ray Diffraction Technique (XRD) from a scanning angle of 20°–80° at a scanning rate of 2° per minute. The thermal stability of the product was measured using Thermo Gravimetric Analysis (TGA) techniques at temperatures ranging from 30 to 900°C. For calculating granular particle size, transmission electron microscopy was used. The structure and the element analysis were done using Scanning Electron Microscopy (SEM), Energy Dispersive Spectroscopy (EDS), and X-Ray Fluorescence (XRF) for fluorescence emission activity. The magnetic characteristics of the material were determined by using a vibrating sample magnetometer (VSM) at room temperature, and photocatalytic activity resulted from the degradation of methyl orange dye only.

2.1 | Optical study

The optical properties were studied from the UV visible spectrum. The silica-supported magnesium ferrite nanorods were soluble in a very low concentration of hydrochloric acid. The resulting solution was analyzed,
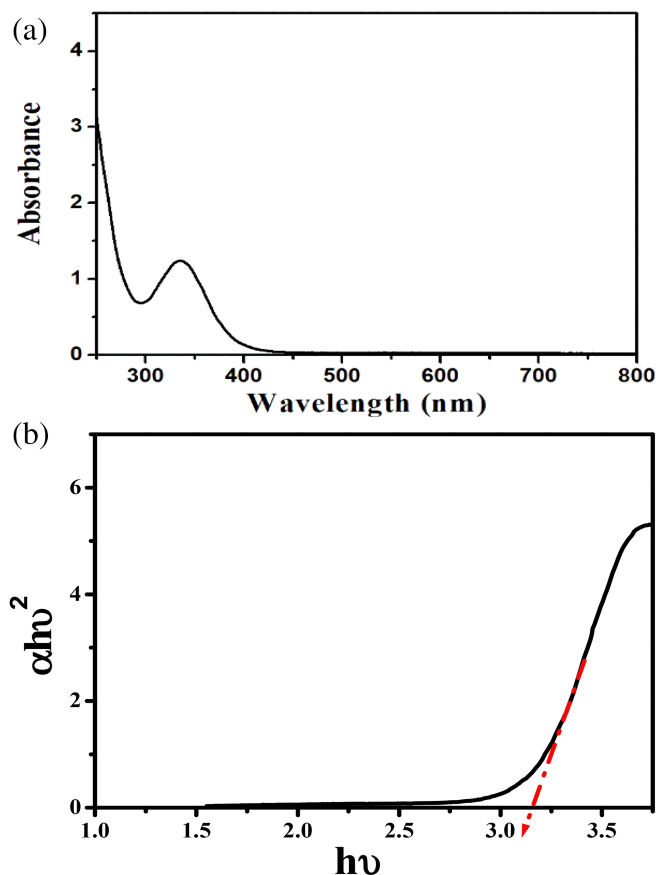
FIGURE 1 (a) UV visible spectra of MgFe$_2$O$_4$@SiO$_2$ nanorods; (b) TAUC plot ofMgFe$_2$O$_4$@SiO$_2$ nanorods

FIGURE 2 XRD spectrum of MgFe$_2$O$_4$@SiO$_2$ nanorods

ranging from 200–800 nm at maximum absorption of ~334 nm, as shown in Figure 1a. The corresponding band gap for MgFe$_2$O$_4$@SiO$_2$ was estimated by using the TAUC plot of 3.1 eV shown in Figure 1b. The band gap calculated by Tauc's plot relationship is expressed as follows:

$$(\alpha h\upsilon)^{1\backslash n} = C\left(h\upsilon - E_g\right) \qquad (1)$$

where α = the absorption coefficient, ν = frequency ($\nu = c/\lambda$, h is Planck's constant, λ = wavelength, c = speed oflight,) n = 2 for direct optical band gap, respectively, C = proportionality constant and E_g = band gap.[54]

2.2 | X – ray diffractometry

In Figure 2, the XRD spectrum of silica-supported magnesium ferrite nanorods shows intense peaks corresponding to the (hkl) planes at (100), (311), (220), (400), (422), (440) at 25.10°, 37.7°, 47.9°, 53.6°, 62.4°, 70.2°, 75.1°, etc indicating the formation of FCC structure without any impurity.
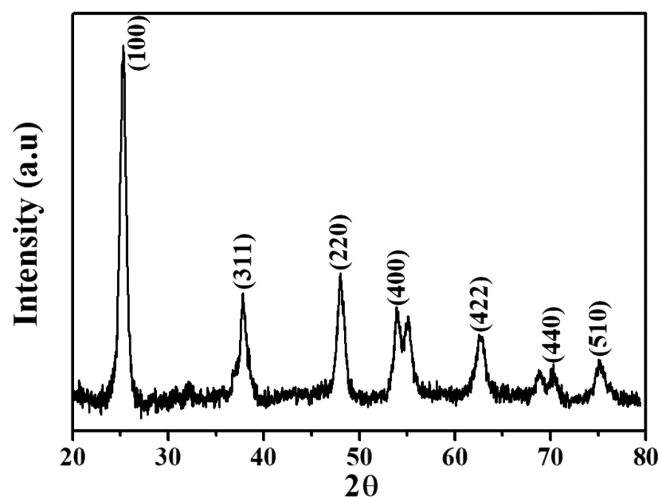
The amorphous silica layer in MgFe$_2$O$_4$@SiO$_2$ magnetic nanorods[39] demonstrated the peak (100) at $2\theta = 25.1°$. When compared to Salunkhe et al.,[39] The XRD pattern reveals that it exhibits an XRD shift of a few degrees because of the change in binding energy between MgFe$_2$O$_4$ and the silica layer. The obtained result through the following relation[24]:

$$a = d\sqrt{N} \qquad (2)$$

where "a" is lattice constant, "d" is interplanar spacing and

$$\sqrt{N} = \sqrt{\left(h^2 + k^2 + l^2\right)} \qquad (3)$$

The volume (V) is calculated by using the following relation:

$$V = a^3 \qquad (4)$$

The X-ray density "dx" was calculated by using the following relation:

$$dx = \frac{8M}{N_A V} \qquad (5)$$

where M = molecular weight, N_A = Avogadro's Number, V = volume of sample.

The broad diffraction peaks exhibit the fine particle nature of ferrite powders. The average crystalline diameter "D_{XRD}" of the prepared samples was obtained from the peak (311) peak of XRD by using the Scherer relation:
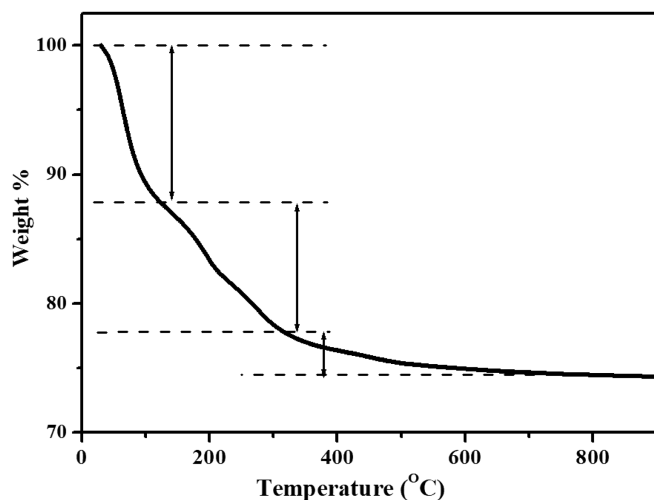
FIGURE 3 TGA spectrum of MgFe$_2$O$_4$@SiO$_2$ nanorods

FIGURE 4 VSM spectrum of MgFe$_2$O$_4$@SiO$_2$ nanorods

$$D_{\text{XRD}} = \frac{k\lambda}{\beta \cos \theta} \qquad (6)$$

where D = Particle Size, k = Constant (0.9), λ = Wavelength of incident X-rays, β = Full Width of Half Maxima (FWHM in radians), θ = Bragg's angle.

The average particle size of the material is 36 nm. The results were compared to the MgFe$_2$O$_4$@SiO$_2$ standard.[47] The inter-planar distance (d): 1.259 Å, the lattice constant (a):1.32 Å, volume (V): 2.30 Å, and the X-Ray density (d_x): 23.60 $\times 10^{-24}$ g/cm^3 and the ion hopping length of the tetrahedral: 4.70 Å sites(L$_A$) and octahedral: 5.75 Å(L$_B$). A spinel phase is observed in MgFe$_2$O$_4$@SiO$_2$ nanorods due to cubic close-packed oxides with eight tetrahedral and four octahedral sites per formula unit.

2.3 | Thermo-gravimetric analysis

Thermogravimetric analysis (TGA) can provide additional quantitative evidence on the structure of the nanoparticle coatings. It is an extremely valuable technique for the surface characterization of nanorods. It allows us to determine the bonding strength of the nanoparticle surface and its stability.[27] The resulting powder sample of MgFe$_2$O$_4$@SiO$_2$ was examined by TGA for the removal of impurities and observed that the initial decomposition of MgFe$_2$O$_4$@SiO$_2$ is between 30 and 150°C due to the removal of absorbed water and the initial loss is 12%. The second decomposition indicates that the temperature difference between 151 and 250°C is primarily due to the loss of other residuals and any impurity during synthesis, namely an excess of chlorides and nitrites, with a secondary loss of 10%. The final decomposition exhibits the
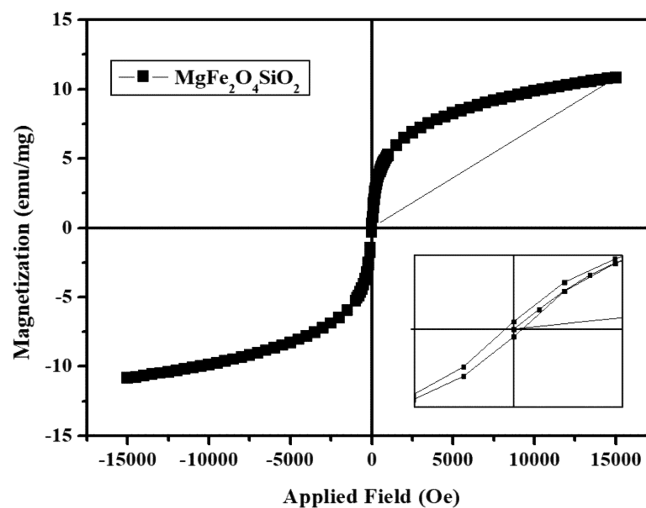
formation of metal oxide between 260°C and 900°C and the final loss is 1.7% in mass fraction as shown in Figure 3. Thus, the synthesized material shows 76% thermal stability at a 600°C temperature. So, the samples were calcined at a temperature of 600°C.

2.4 | Magnetic study

It is important that the core-shell material has super paramagnetic properties while magnetic hysteresis measurements were performed for MgFe$_2$O$_4$@SiO$_2$ in an applied magnetic field.[2,31] The sample was shown to behave like soft magnetic materials with low hysteresis loss. The magnetic hysteresis loop for the sample was completely reversible. Among the most important properties of soft magnetic nanoparticles is saturation magnetization.[38] Magnetic nanoparticles with superior magnetic characteristics might be improved and applied more effectively.[40] Extrapolation in a graph of M versus $1/H$ reveals the saturation magnetization, It has a magnetic saturation (M_s) of 11.38 emu/mg, a magnetic remanence (M_r) of 7.76 emu/mg, a coercivity (H_c) of 23.49 Oe, and an anisotropy constant (K) of 3.14 erg/cm^3. The nanorods observed a high level of permeability magnetization, which was appropriate for the magnetic separation shown in Figure 4. The magnetic moment was found to be 1.19 B using the M versus H measurements. This indicates that the magnesium nanorods are suitable for a wide range of technological applications requiring temperatures greater than room temperature, such as medical applications requiring local hyperthermia, such as at cancer spots.[36] The Bohr magnetization was calculated by using the following formula:
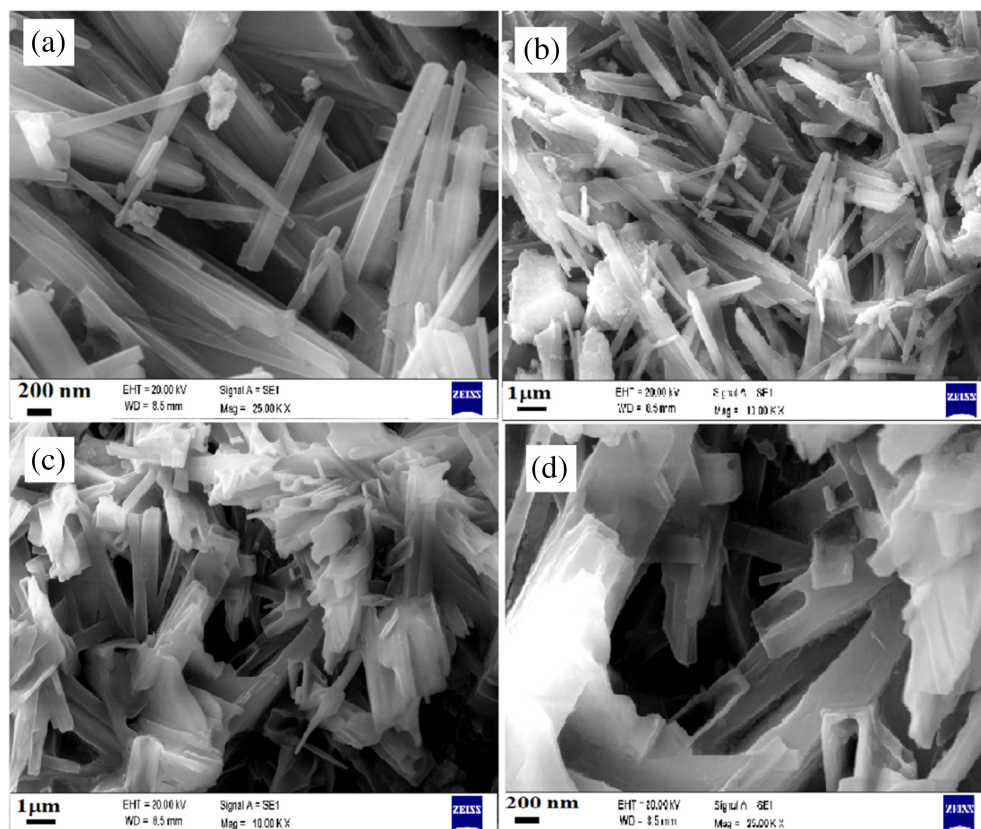
$$\mu_B = \frac{M \times M_s}{5585} \qquad (7)$$

where μ_B = Bohr magneton, M = total molecular weight of composition, M_s = Saturation Magnetization.

2.5 | Field emission scanning electron microscopy and energy dispersive X-ray spectroscopy

The FE-SEM technique can detect and analyze surface topographical, morphological, and compositional properties of micro and nanostructures. The morphology of synthesized materials was studied by the FE-SEM technique.[60] As Figure **5** shows, the FE-SEM images display that the MgFe$_2$O$_4$@SiO$_2$ nanorods were produced with a uniform particle size distribution and highly formed into a uniform rod shape. Figure **5**a,d are shown at 200 nm and Figure **5**b,c at 1 μm in size.

Figure **6** shows the chemical purities and elemental composition of the MgFe$_2$O$_4$@SiO$_2$ materials produced by energy dispersive X-ray analysis (EDS), the existence of Mg, O, Fe, and Si was determined by their corresponding peaks. There is no other peak that indicates MgFe$_2$O$_4$@SiO$_2$ does not contain any impurity. Hence, the synthetic material is pure. The presence of all elements and their atomic percentage and weight percentage are listed in Table **1** below.
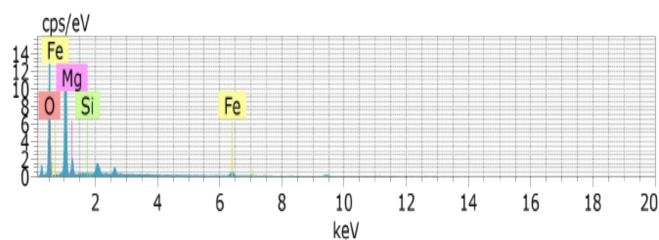

FIGURE 6   EDS spectrum of MgFe$_2$O$_4$@SiO$_2$ nanorods

TABLE 1   The elemental composition of MgFe$_2$O$_4$@SiO$_2$ nanorods

Sr.no.	Elements	Weight %	Atomic %
1.	O	60.48	82.30
2.	Mg	2.94	2.63
3.	Si	2.12	1.64
4.	Fe	34.46	13.43
	Total	100	100

2.6 | High-resolution transmission electron microscopy

In Figure **7**, an HR-TEM image of MgFe$_2$O$_4$@SiO$_2$ synthesized at 500°C is presented. In terms of morphology and crystallite size, the silica-supported magnesium ferrite nanorods produced by the co-precipitation methodology

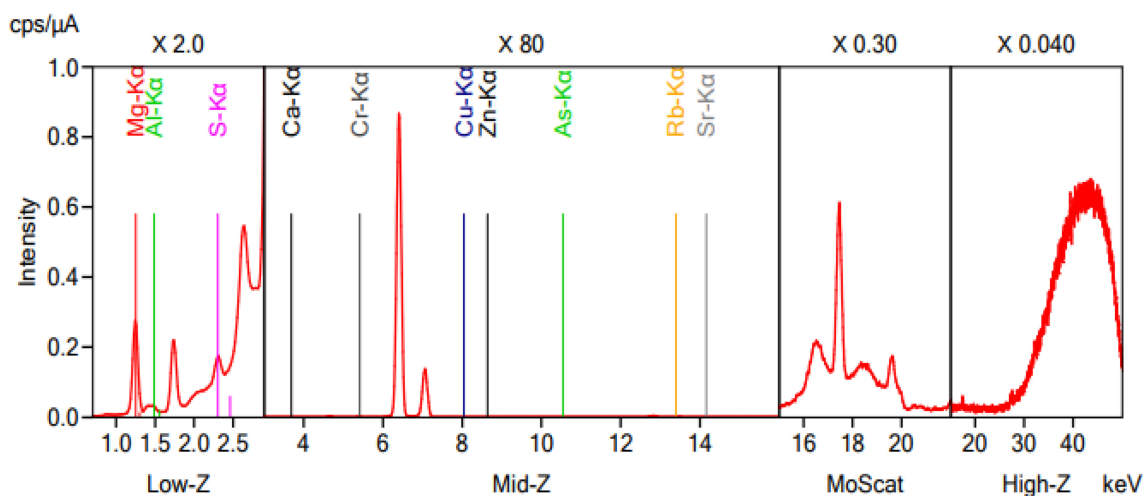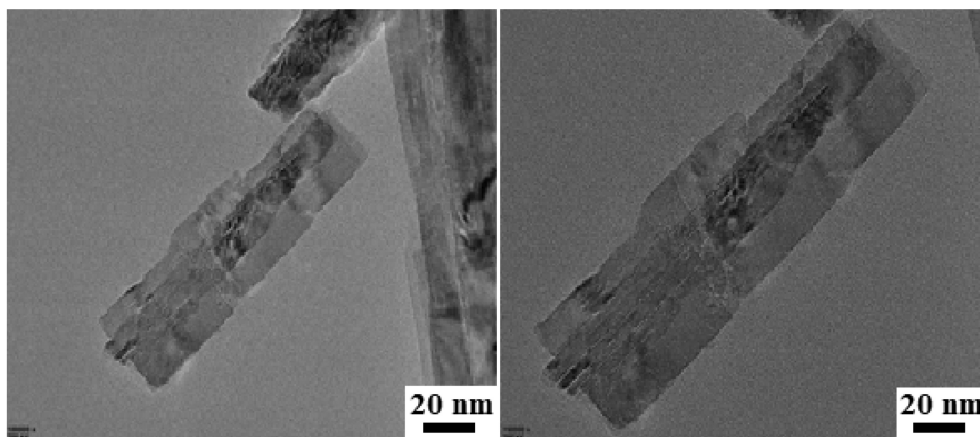**FIGURE 7** HR-TEM of MgFe$_2$O$_4$@SiO$_2$ nanorods (20 nm for both images)

FIGURE 8 XRF plot of MgFe$_2$O$_4$@SiO$_2$ nanorods

were uniform. The rod size in the 36 nm, shape structure of MgFe$_2$O$_4$@SiO$_2$ shown in FE-SEM was confirmed by HR-TEM images.

2.7 | X-ray fluorescence

As a result of fluorescence properties, the emission intensity peaks for elemental composition of synthesized MgFe$_2$O$_4$@SiO$_2$ nanorods indicate that the metal and its oxides are the emission intensity peak at 2.332 cps/µA indicates the presence of Fe$_2$O$_3$, for MgO at 0.236 cps/µA and for silicate at 0.0927 cps/µA. Hence, it determines the presence of Mg, Fe, and SiO$_2$ elements in the MgFe$_2$O$_4$@SiO$_2$ nanorods shown in Figure 8 and Table 2 below.

2.8 | Photocatalytic degradation

The silica-supported Magnesium Ferrite Nanorods demonstrated catalytic activity by photocatalytically degrading

TABLE 2 Elemental composition regarding to XRF data

Sr. no	Material	Elemental composition			Total
		Fe$_2$O$_3$	MgO	SiO$_2$	
1.	MgFe$_2$O$_4$@SiO$_2$	84.20	15.0	0.8	100%

Methyl Orange. Figure 9a depicts the UV–Visible absorption spectra of methyl orange dye in the suspension of MgFe$_2$O$_4$@SiO$_2$ nanocomposites with respect to irradiation time. As can be seen from the figure, the characteristic absorption peak of methyl orange dye at ~485 nm decreases gradually with respect to time irradiation. The complete degradation of methyl orange dye has been observed within 270 min by using MgFe$_2$O$_4$@ SiO$_2$ nanocomposite.

The plausible mechanism[55,61] is as follows,

Figure 9b depicts a kinetic plot of the methyl orange photo degradation reaction for various catalysts with respect to varying irradiation times. The control of experiments reveals that the concentration of methyl orange has been constant in the absence of photocatalysts in the

presence of sunlight, suggesting that methyl orange dye is very stable photochemically. Within an irradiation time of 270 min., the complete degradation of methyl orange is observed for 30 mol% $MgFe_2O_4@SiO_2$ composites, while less degradation was observed for without catalyst, 20, and 10 mol% $MgFe_2O_4@SiO_2$ composites, respectively, and hence it reveals that $MgFe_2O_4@SiO_2$ required less time to degrade methyl orange completely to that of other composites. This observation indicates that the photocatalytic degradation reaction of the composite is highly dependent upon the amount of $MgFe_2O_4@SiO_2$ nanocomposite. Furthermore, $MgFe_2O_4@SiO_2$ catalyst has a higher photo response and fluorescence in visible light, as it shows more absorption in the visible region with the lowest band gap of about 3.1 eV.

Figure 9c shows the plot of lnC_0/C of methyl orange dye in the suspension of all samples with irradiation time. The linear nature of the graph of lnC_0/C of all samples with respect to irradiation time suggests that photocatalytic degradation is first order. It is visibly observed that the color of the Methyl Orange solution gradually changes from orange to light orange and finally to colorless.

The kinetic study shown as follows,[58,61]

$$\ln\left(C_o/C\right) = kt.$$

where C_o = Initial concentration, C = Final concentration, k = rate constant and t = time. It can be calculated from the simulation curve as shown in Figure 9c. The rate of degradation was monitored by using UV – Visible Spectroscopy and the degradation efficiency was calculated by using formula[56]:

$$\text{Degradation efficiency}\,(\%) = \frac{C_o - C}{C_o} \times 100.$$

C_o and C are the dye concentration at initial and various times.

The $MgFe_2O_4@SiO_2$ nanorods catalyzed degradation shows 79% Degradation Efficiency of methyl orange dye.

2.9 | Catalyst recyclability

Reusability of the prepared $MgFe_2O_4@SiO_2$ is one of the most significant features for catalyst efficiency over practical reuses. Therefore, 3 cycles of photocatalytic degradation of methyl orange were carried out using $MgFe_2O_4@SiO_2$ under sunlight as shown in Figure 10. The efficiency of the catalyst is measured by the total number of catalytic cycles while maintaining the catalytic activity.[60] The catalyst's outstanding efficiency was demonstrated after 3 cycles, confirming the stability of the synthesized catalysts.
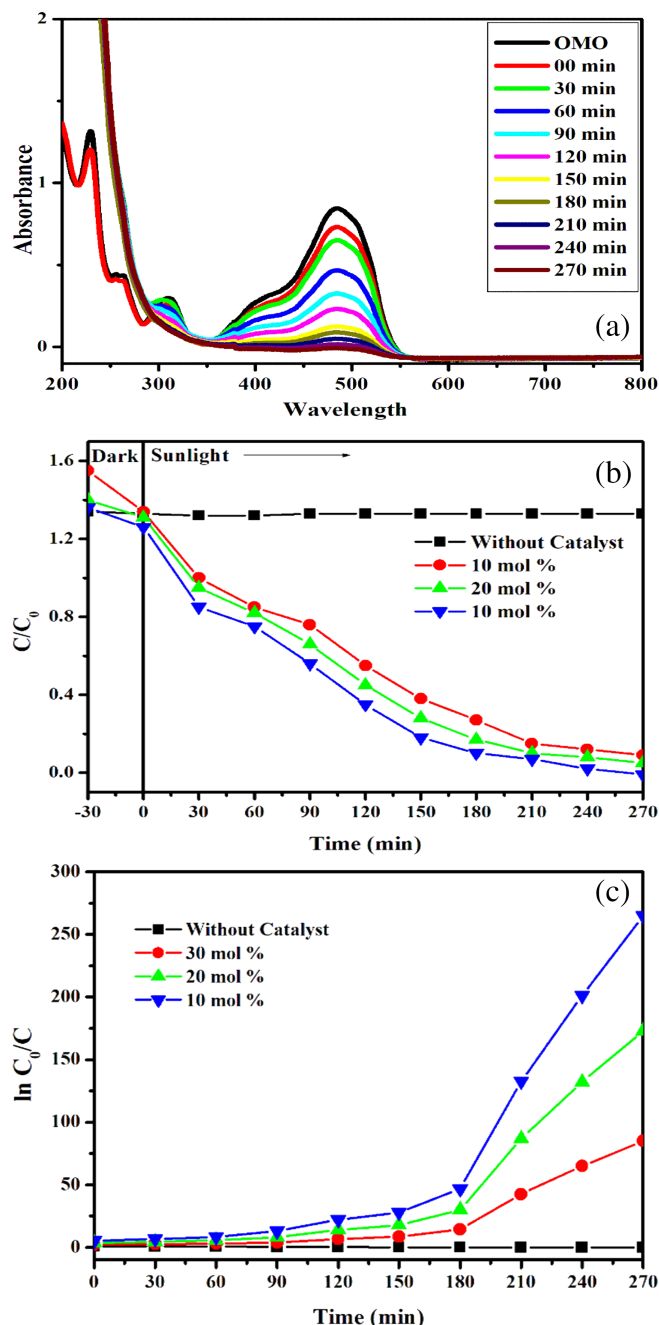

FIGURE 9 (a) Optical absorption spectra of methyl orange. (b) Kinetic plot of methyl orange photo degradation reaction. (c) Corresponding plot of ln C_0/C versus time

2.10 | BET analysis

The surface area and porosity of the $MgFe_2O_4@SiO_2$ nanorods were measured using the Brunauer–Emmett–Teller (BET) equation following the Barrett–Joyner–Halanda (BJH) method. Figure 11 shows (a) BET surface area and inset, and (b) pore size distribution From the N_2 adsorption–desorption isotherm, the BET surface area of the nanorods is 19.297 $m^2\,g^{-1}$, total pore volume at P/Po
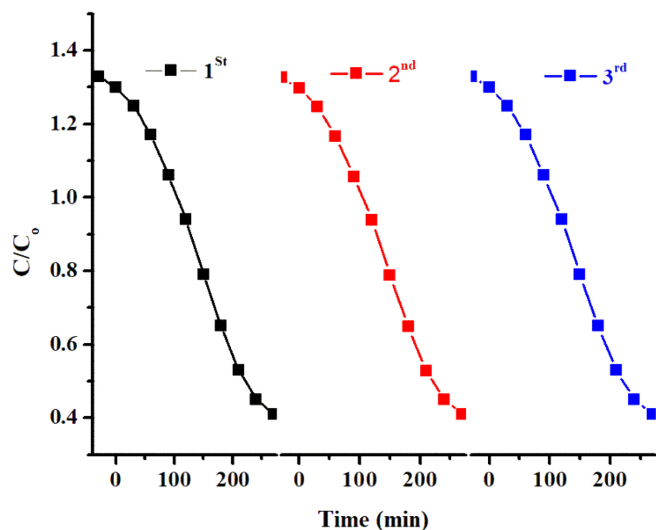
FIGURE 10 Catalyst recyclability

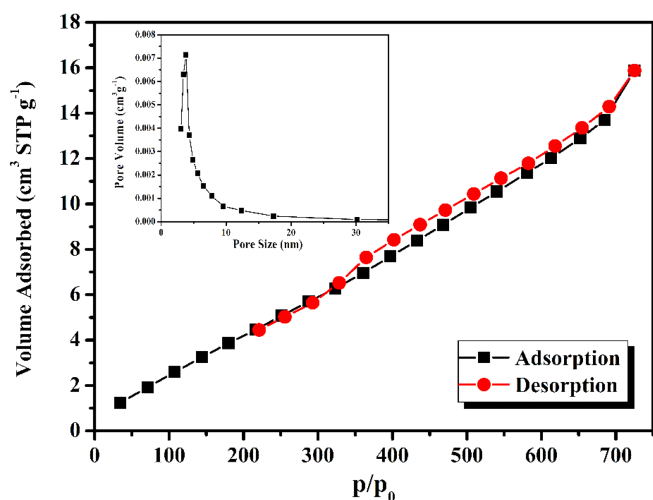**FIGURE 11** (a) BET surface area and inset, (b) pore size distribution of $MgFe_2O_4@SiO_2$ nanorods

(0.99) is 2.46 cm^3g^{-1} and the average pore diameter was found to be 5.10 nm. The isotherm represents type (V), with an H_3 hysteresis loop, which is a characteristic of mesoporous materials. This mesoporous material was evident from the adsorption of water molecules on the surface.[59]

3 | EXPERIMENTAL PROCEDURE

3.1 | Chemicals

Himedia analytical grade magnesium perchlorate $(MgClO_4)_2$, ferric nitrate Fe $(NO_3)_3.9H_2O$, reducing agent hydrazine hydrate (99.99% purity), and Tetra ethyl ortho silicate (TEOS) were all purchased. The experiment was performed using distilled water as the green solvent. The silica-supported magnesium ferrites $(MgFe_2O_4@SiO_2)$ were synthesized by the coprecipitation method.

3.2 | MgFe$_2$O$_4$ nanorod synthesis

The magnesium perchlorate and ferric nitrate were taken in 1:2 M proportions in a round-bottom flask. The reaction was stirred up to a homogenous mixture. After obtaining the transparent solution, the stoichiometric amount of hydrazine hydrate was added to the reaction mixture and continuously stirred for 4 hr to maintain pH = 09 at room temperature and provide excellent precipitates. The reducing agent, Hydrazine Hydrate, was used to maintain the pH. Then the precipitate was filtered and washed several times with mild hot distilled water and then ethanol to make the precipitate free from chlorides and impurities. Then the dried crude product was calcinated at 600°C for 3 hr. The obtained brown-colored precipitate is made of spinel $MgFe_2O_4$ nanorods.

3.3 | Silica-supported MgFe$_2$O$_4$ nanorod synthesis

For half an hour, $MgFe_2O_4$ (1.0 g) was stirred in an ethanol-water system (4:1) for half an hour. Then the reaction was continuously stirred along with the addition of hydrazine hydrate (2 mL) followed by the dropwise addition of Tetra Ethyl Ortho Silicate (TEOS) (1.5 mL). Then the reaction mixture was continuously stirred for 8 hr at room temperature. And finally, the precipitate was washed several times with water. The dried product was collected and calcinated at 500°C for 6 hr to finally collect the $MgFe_2O_4@SiO_2$ nanorods.

3.4 | Photocatalytic degradation study

The 25-ppm solution of methyl orange was prepared and taken as the first sample. Then it was continuously stirred in the dark for 30 min and taken as a second sample. The stoichiometric amount of $MgFe_2O_4@SiO_2$ was added and then the reaction was exposed to sunlight up to complete degradation. The degradation was completed within 270 min.

4 | CONCLUSIONS

The $MgFe_2O_4@SiO_2$ nanorods have been successfully synthesized by using the co-precipitation method. The

size of mesoporous nanorods is 36 nm and the optical band gap is 3.1 eV, corresponding to a ~ 334 nm wavelength. The TGA shows the 74% thermal stability of the material. The VSM shows sufficient magnetization with a 1.19B magnetization value. The $MgFe_2O_4@SiO_2$ is rod shaped and is confirmed by FE-SEM and HR-TEM images. The XRF emission plot indicates the presence of all elements in the composition of $MgFe_2O_4@SiO_2$. $MgFe_2O_4@SiO_2$ was successfully used for the complete photocatalytic degradation of methyl orange dye in 270 minutes. The absorption peak of degradation is shown at ~485 nm. Within the various compositions of the catalyst, 30 mol% $MgFe_2O_4@SiO_2$ shows complete degradation. As a result, these nanorods show complete photocatalytic degradation of methyl orange dye within 270 nm. The catalyst $MgFe_2O_4@SiO_2$ is highly magnetic, and it has been shown to have nearly similar efficiency over 3 cycles and shows degradation efficiency of about 79%. The BET analysis shows the surface area, pore volume, and pore diameter are 19.2 m^2 g^{-1}, 2.46 cm^{3}g^{-1}, and 5.10 nm, respectively.

ACKNOWLEDGMENT

ORCID

Radhakrishnan M. Tigote https://orcid.org/0000-0001-5350-9140

REFERENCES

[1] Y. A. Barnakov, M. H. Yu, *Langmuir* **2005**, *21*, 7524.

[2] Y. Ichiyanagi, M. Kubota, S. Moritake, Y. Kanazawa, T. Yamada, T. Uehashi, *J. Magnet. Magnet. Mater.* **2007**, *310*, 2378.

[3] C. Lin, Y. Li, M. Yu, P. Yang, J. Lin, *Adv. Funct. Mater.* **2007**, *17*, 1459.

[4] S. Andreescu, J. Njagi, C. Ispas, Chapter 7 - nanostructured materials for enzyme immobilization and biosensors. in *The new Frontiers of organic and composite nanotechnology* (Eds: V. Erokhin, M. K. Ram, O. Yavuz), Elsevier, Amsterdam **2008**, p. 355. https://doi.org/10.1039/B811063H.

[5] S. A. Bocanegra, A. D. Ballarini, O. A. Scelza, S. R. de Miguel, *Mater. Chem. Phys.* **2008**, *111*, 534.

[6] L. Xu, W. Zou, J. Hong, *Sci. Ed.* **2009**, *24*, 354.

[7] F. Wang, S. Hu, *Microchim. Acta* **2009**, *165*, 1.

[8] F. Zhu, C. Li, H. Fan, *J. Nat. Gas Chem.* **2010**, *19*, 169.

[9] A. Franco, V. S. Zapf, V. B. Barbeta, R. F. Jardim, *J. Appl. Phys.* **2010**, *107*, 73904. https://doi.org/10.1063/1.3359709.

[10] A. Franco, M. S. Silva, *J. Appl. Phys.* **2011**, *109*, 7B505. https://doi.org/10.1063/1.3536790.

[11] S. B. Kalidindi, B. R. Jagirdar, *ChemSusChem* **2012**, *5*, 65.

[12] I. Natali Sora, T. Caronna, F. Fontana, C. de Julián Fernández, A. Caneschi, M. Green, *J. Solid State Chem.* **2012**, *191*, 33.

[13] M. Kaya, M. Zahmakıran, S. Özkar, M. Volkan, *ACS Appl. Mater. Interfaces* **2012**, *4*, 3866.

[14] S. Gaur, D. Pakhare, H. Wu, D. J. Haynes, J. J. Spivey, *Energy Fuels* **2012**, *26*, 1989.

[15] I. Sharifi, H. Shokrollahi, S. Amiri, *J. Magnet. Magnet. Mater.* **2012**, *324*, 903.

[16] D. Chen, D.-Y. Li, Y.-Z. Zhang, Z.-T. Kang, *Ultrason. Sonochem.* **2013**, *20*, 1337.

[17] M. Rahimzadeh, H. Eshghi, F. Moeinpour, M. Bakavoli, *Chin. J. Catal.* **2014**, *35*, 376.

[18] M. Reza Barati, C. Selomulya, K. Suzuki, *J. Appl. Phys.* **2014**, *115*, 17B522. https://doi.org/10.1063/1.4867751.

[19] S. K. Kazi, R. M. Tigote, G. B. Tiwari, K. P. Haval, R. N. Adude, *Int. J. Curr. Eng. Sci. Res.* **2019**, *6*, 931.

[20] M. A. Almessiere, Y. Slimani, S. Guner, M. Sertkol, A. Demir Korkmaz, S. E. Shirsath, A. Baykal, *Ultrason. Sonochem.* **2019**, *58*, 104654. https://doi.org/10.1016/j.ultsonch.2019.104654.

[21] M. A. Almessiere, Y. Slimani, S. E. Shirsath, Y. S. Wudil, A. Baykal, I. Ercan, *Results Phys.* **2020**, *19*, 103350. https://doi.org/10.1016/j.rinp.2020.103350.

[22] H. Das, N. Sakamoto, H. Aono, K. Shinozaki, H. Suzuki, N. Wakiya, *J. Magnet. Magnet. Mater.* **2015**, *392*, 91.

[23] I. G. Blanco-Esqueda, G. Ortega-Zarzosa, J. R. Martínez, A. L. Guerrero, *Adv. Mater. Sci. Eng.* **2015**, *2015*, 678739. https://doi.org/10.1155/2015/678739.

[24] M. Bagheri, M. A. Bahrevar, A. Beitollahi, *Ceram. Int.* **2015**, *41*, 11618.

[25] R. Benrabaa, A. Löfberg, J. Guerrero Caballero, E. Bordes-Richard, A. Rubbens, R.-N. Vannier, H. Boukhlouf, *A. Barama* **2015**, *58*, 127.

[26] A. Bayat, M. Shakourian-Fard, N. Ehyaei, M. Mahmoodi Hashemi, *RSC Adv.* **2015**, *5*, 22503.

[27] C. O. Ehi-Eromosele, B. I. Ita, E. E. J. Iweala, K. O. Ogunniran, J. A. Adekoya, T. O. Siyanbola, *J. Nano Res.* **2016**, *40*, 146.

[28] N. U. Ain, W. Shaheen, B. Bashir, N. M. Abdelsalam, M. F. Warsi, M. A. Khan, M. Shahid, *Ceram. Int.* **2016**, *42*, 12401.

[29] M. A. Almessiere, S. Güner, Y. Slimani, A. Baykal, S. E. Shirsath, A. D. Korkmaz, R. Badar, *J. Mol. Struct.* **2022**, *1248*, 131412. https://doi.org/10.1016/j.molstruc.2021.131412.

[30] M. A. Amer, T. Meaz, S. Attalah, F. Fakhry, *J. Magnet. Magnet. Mater.* **2016**, *401*, 150.

[31] O. Kaman, T. Dědourková, J. Koktan, J. Kuličková, M. Maryško, P. Veverka, R. Havelek, K. Královec, K. Turnovcová, P. Jendelová, A. Schröfel, L. Svoboda, *J. Nanopart. Res.* **2016**, *18*, 100.

[32] S. Mallesh, D. Prabu, V. Srinivas, *AIP Adv.* **2017**, *7*, 56103. https://doi.org/10.1063/1.4975355.

[33] H. Das, N. Debnath, A. Toda, T. Kawaguchi, N. Sakamoto, H. Aono, K. Shinozaki, H. Suzuki, N. Wakiya, *Adv. Powder Technol.* **2017**, *28*, 1696.

[34] O. Kaman, J. Kuličková, M. Maryško, P. Veverka, V. Herynek, R. Havelek, K. Královec, D. Kubániová, J. Kohout, P. Dvořák, Z. Jirák, *IEEE Trans. Magnet.* **2017**, *53*, 1.

[35] K. Alexander, H. Das, N. Wakiya, A. Valiullin, *Phys. Solid State* **2018**, *60*, 1752.

[36] M. A. Almessiere, Y. Slimani, S. Rehman, F. A. Khan, Ç. D. Güngüneş, S. Güner, S. E. Shirsath, A. Baykal, *Arab. J. Chem.* **2020**, *13*, 7403.

[37] T. Dippong, E. A. Levei, O. Cadar, *J. Chem.* **2017**, *2017*, 7943164. https://doi.org/10.1155/2017/7943164.

[38] R. P. Singh, C. Venkataraju, *Chin. J. Phys.* **2018**, *56*, 2218.

[39] N. Salunkhe, C. Ladole, N. Thakare, A. Aswar, *Res. Chem. Intermediat.* **2018**, *44*, 355.

[40] L. Zheng, K. Fang, M. Zhang, Z. Nan, L. Zhao, D. Zhou, M. Zhu, W. Li, *RSC Adv.* **2018**, *8*, 39177.

[41] A. Ahmad, H. Bae, I. Rhee, *AIP Adv* **2018**, *8*, 55019. https://doi.org/10.1063/1.5027898.

[42] L. T. T. Nguyen, L. T. H. Nguyen, N. C. Manh, D. N. Quoc, H. N. Quang, H. T. T. Nguyen, D. C. Nguyen, L. G. Bach, *J. Chem.* **2019**, *2019*, 3428681. https://doi.org/10.1155/2019/3428681.

[43] M. Mahmoudzadeh, E. Mehdipour, R. Eisavi, *J. Coordinat. Chem.* **2019**, *72*, 841.

[44] M. Bououdina, B. Al-Najar, L. Falamarzi, J. Judith Vijaya, M. N. Shaikh, S. Bellucci, *Europ. Phys. J. Plus* **2019**, *134*, 84.

[45] H. U. Muhammad Yakob, *AIMS Mater. Sci.* **2019**, *6*, 45.

[46] A. Becker, K. Kirchberg, R. Marschall, *Zeitschrift für Physikalische Chemie* **2020**, *234*, 645.

[47] E. K. Chiwandika, S.-K. Cho, S.-M. Jung, *Minerals* **2020**, *10*, 800. https://doi.org/10.3390/min10090800.

[48] R. Rajendran, R. Muralidharan, R. Santhana Gopalakrishnan, M. Chellamuthu, S. U. Ponnusamy, E. Manikandan, *Europ. J. Inorgan. Chem.* **2011**, *2011*, 5384. https://doi.org/10.1002/ejic.201100840.

[49] S. H. A. Hassan, A. H. Alshamsi, *Biol. Chem. Sci.* **2015**, *6*, 985.

[50] M. Maaza, B. D. Ngom, M. Achouri, K. Manikandan, *Vacuum* **2015**, *114*, 172.

[51] J. Zhang, Q. Huang, J. Du, *Polym. Int.* **2016**, *65*, 1365.

[52] A. Diallo, T. B. Doyle, B. M. Mothudi, E. Manikandan, V. Rajendran, M. Maaza, *J. Magnet. Magnet. Mater.* **2017**, *424*, 251.

[53] A. G. Abraham, A. Manikandan, E. Manikandan, S. Vadivel, S. K. Jaganathan, A. Baykal, P. S. Renganathan, *J. Magnet. Magnet. Mater.* **2018**, *452*, 380.

[54] B. S. H. Hassan, A. Alshamsi, *Asian J. Chem.* **2018**, *30*, 273.

[55] B. S. Hussain, H. A. Alshamsi, *Orient. J. Chem.* **2018**, *34*, 1898.

[56] M. Al-Bedairy, H. Alshamsi, *Eurasian J. Anal. Chem.* **2018**, *13*, em72. https://doi.org/10.29333/ejac/101785.

[57] A. Charles Prabakar, B. Sathyaseelan, G. Killivalavan, B. Iruson, K. Senthilnathan, E. Manikandan, D. Sivakumar, *J. Nanostruct.* **2019**, *9*, 694.

[58] A. C. P. Govindarasu Killivalavan, K. C. B. Naidu, B. Sathyaseelan, G. Rameshkumar, D. S. Krishnamoorthy, *Biointerface Res Appl Chem* **2020**, *10*, 5306.

[59] N. Hussain, S. Alwan, H. Alshamsi, I. Sahib, *Int. J. Chem. Eng.* **2020**, *2020*, 9068358. https://doi.org/10.1155/2020/9068358.

[60] H. Alshamsi, M. Abbas, A Bedairy, S. H. Alwan, IOP Conf. Series: Earth and Environmental Science, *722* (**2021**) 12005. https://doi.org/10.1088/1755-1315/722/1/012005.

[61] Z. H. Abdulhusain, H. A. Alshamsi, M. Salavati-Niasari, *J. Mater. Res. Technol.* **2021**, *15*, 6098.

[62] M. Jarvin, S. A. Kumar, G. Vinodhkumar, E. Manikandan, S. S. R. Inbanathan, *Mater. Lett.* **2021**, *305*, 130750. https://doi.org/10.1016/j.matlet.2021.130750.

[63] P. Paulraj, A. Umar, K. Rajendran, A. Manikandan, A. Sathamraja, R. Kumar, E. Manikandan, K. Pandian, S. Baskoutas, H. Algadi, A. A. Ibrahim, M. A. Alsaiari, *J. Mater. Sci. Mater. Electron.* **2021**, *32*, 8317.

[64] H. Altaee, H. A. Alshamsi, *J. Phys. Conf. Series* **2020**, *1664*, 12074. https://doi.org/10.1088/1742-6596/1664/1/012074.

[65] H. Altaee, H. A. H. Alshamsi, B. A. Joda, *AIP Conf. Proceed.* **2020**, *2290*, 30036. https://doi.org/10.1063/5.0027427.